

An improved mode superposition method applicable to a coupled structural–acoustic system with a multiple cavity

Jin Woo Lee^{a,*}, Jang Moo Lee^b

^a*National Creative Research Initiatives Center for Multiscale Design (311-206), School of Mechanical and Aerospace Engineering, Seoul National University, San56-1 Shinlim-9-dong, Kwanak-gu, Seoul 151-742, Republic of Korea*

^b*School of Mechanical and Aerospace Engineering, Seoul National University, San 56-1, Shillim-dong, Kwanak-gu, Seoul 151-742, Republic of Korea*

Received 12 June 2006; received in revised form 4 September 2006; accepted 28 October 2006

Available online 13 December 2006

Abstract

This paper proposes an advanced analytical method that can be used to obtain acoustical modal properties of multiple three-dimensional (3D) cavities, where cavities are connected in series by necks. The method can also be used to obtain the modal properties of a 3D coupled structural–acoustic system including the multiple cavities. The proposed method uses evanescent waves, not considered in previous mode superposition methods, as well as standing waves as basis functions because of discontinuity in the cross-sectional area of a cavity and a neck. Evanescent waves are converted to the added length term of a neck in developing the governing equations. Therefore, the neck's effective length, which consists of the physical length and the added length, is used in the characteristic matrix of the governing equation instead of the physical length of the neck. The effective length term increases the exactness of the natural frequencies of the 3D systems of interest and becomes a new control parameter for a coupled system because the evanescent waves can account for the effect of the neck's position on multiple cavities. The proposed method is validated by application to one 3D double cavity where two cavities are connected by a neck and three 3D coupled systems including the double cavity. Also, the relative position of the plate and the acoustic pressure distribution of a double cavity are examined for their effect on the degree of coupling. © 2006 Elsevier Ltd. All rights reserved.

1. Introduction

In the last few decades, coupled structural–acoustic systems have been identified in many ways. Experiments have revealed physical phenomena that have forced researchers to consider structural–acoustic coupling interaction using analytical approaches. Thereafter, an exact governing equation describing the dynamic characteristics of a coupled system was derived. Since the mode superposition method, used in structural modeling for dynamics, was extended to the combined system, it has been widely used to obtain governing equations [1]. Also, coupling parameters, representing the degree of coupling of a coupled system, were derived in various forms [2–5]. Since they have generally been expressed using basis functions for uncoupled structural and acoustic systems, the choice of what types of functions to use as the basis functions is crucial.

*Corresponding author. Tel.: +82 2 880 1597; fax: +82 2 880 5431.

E-mail addresses: jw062nam@yahoo.co.kr, jw062@hanmir.com (J.W. Lee).

Nomenclature	
A_{d^s}, A_{d^e}	coefficients of the rigid-walled acoustic mode and of the decaying wave, respectively
$c_i A_{d_i^s}$	coefficient of the d_i^s th rigid-walled acoustic mode in the i th acoustic cavity
B_m	coefficient of in vacuo natural mode of the plate
$s_j B_{m_j}$	coefficient of the m_j th in vacuo natural mode of the j th plate
$c_i C_{m_i^n}$	coefficient of cross-mode in the i th acoustic cavity
c	sound speed
D_E	plate flexural rigidity
E	Young's modulus of elasticity
$\tilde{f}(\vec{r}_s, t)$	external transverse load per unit area at \vec{r}_s
$y g_n$	distance between centers of a neck and a cavity in the y -direction
$z g_n$	distance between centers of a neck and a cavity in the z -direction
HF	product of two Heaviside functions H
h_i	a half of height of the i th acoustic cavity
h_n	a half of height of the neck
j	imaginary unit ($= \sqrt{-1}$)
k	wavenumber
${}_c k_{d^s}$	$= {}_c \omega_{d^s} / c$
l_n	real length of a neck
l'_n	effective length of a neck
Δl_n	total added length ($= \Delta l_1 + \Delta l_2$)
Δl_i	added length created by an evanescent wave in the i th acoustic cavity
$\dot{m}(\vec{r}, t)$	net influx of the mass per unit time
m_{c_i}	net influx of the mass in the i th acoustic cavity
$\tilde{p}(\vec{r}, t)$	acoustic pressure
$s \tilde{p}(\vec{r}_s, t)$	acoustic pressure applied to the plate at \vec{r}_s
$\tilde{p}^s(r, t)$	standing wave
$\tilde{p}^e(r, t)$	evanescent wave or decaying wave
$p_{c_i}^e(\vec{r})$	evanescent wave in the i th acoustic cavity
q_{g_i}	magnitude of a regular flow input
\vec{r}	position vector in the cavity
\vec{r}_{d_i}	position vector at the interface between a cavity and a neck
\vec{r}_s	position vector on the plate
\vec{r}_{s_j}	a point on the j th plate
\vec{r}_{g_i}	vector representing the position of a regular flow in the i th acoustic cavity
S_i	cross-sectional area of each cavity ($i = 1, 2$) and a neck ($i = n$)
t_s	plate thickness
$\vec{u}(\vec{r}, t)$	particle velocity
w_i	a half of width of the i th acoustic cavity
w_n	a half of width of the neck
<i>Greek symbols</i>	
α_{d^e}	decay rate of an evanescent wave
$\delta(\vec{r})$	Dirac delta function ($=$ the unit impulse function)
ρ_a	density of the acoustic medium
ρ_s''	area density of the plate
Θ_{d^e}	d^e th cross-mode
ν	Poisson's ratio
$\tilde{\zeta}(\vec{r}_s, t)$	structural displacement at \vec{r}_s
$\tilde{\zeta}_n(t)$	displacement of the lumped mass in a neck
$\psi_{d^s}^s$	d^s th rigid wall acoustic mode
$\psi_{d^e}^e$	decaying wave with the d^e th cross-mode
ψ_m	in vacuo natural mode of the plate
$c_i \psi_{d_i^s}^s$	the d_i^s th rigid wall acoustic mode in the i th acoustic cavity
$s_j \psi_{m_j}$	the m_j th in vacuo natural mode of j th the plate
ω	angular frequency
${}_c \omega_{d^s}$	d^s th natural angular frequency of the cavity
$s \omega_m$	m th natural angular frequency of the plate
<i>Subscripts</i>	
c_i	the i th acoustic cavity
s_j	the j th plate
n	neck

The basis functions represent the dynamic characteristics of each uncoupled system. In this paper, governing equations are derived using new basis functions for a coupled structural–acoustic system with multiple cavities, where cavities are connected in series by necks. The effect of the neck's position on the modal properties of a double cavity and a coupled structural–acoustic system with the double cavity is investigated.

Mode superposition methods have been useful for determining the natural frequencies of coupled structural–acoustic systems. The methods are especially useful in a low frequency range, where the wavelength of interest is greater than, or of the same order as, the dimensions of the cavities [6]. Wolf used the modal synthesis technique to describe the dynamics of a combined structural–acoustic system [1]. His formulation was used to obtain economically the system eigenvalues and eigenvectors. Ma and Hagiwara derived an improved mode-superposition technique using the new quasi-static compensation technique and calculated a more accurate modal frequency response (MFR) of a coupled structural–acoustic system [7]. Using the mode superposition method, Luo and Gea proposed an analytical modal sensitivity analysis method for a coupled structural–acoustic system to calculate the sensitivities of the eigenvalues and eigenvectors [8]. Hong and Kim have applied the modal expansion method, including the concept of an equivalent mass source, to solve the dynamic equations of a coupled structural–acoustic system [2,9,10]. Sung and Nefske developed the finite element formulation representing the structure of a vehicle and its enclosed acoustic cavity to identify roles of the structural and acoustic mode in the vibration-induced response [11].

Similarly, Slepnyan and Sorokin presented a formulation of the boundary integral equation method for the analysis of vibrations of composite thin-walled structures in an acoustic medium [12]. Chen et al. presented a theoretical formulation on the collocation method for the eigenanalysis of arbitrarily shaped acoustic cavities using the imaginary-part kernel [13].

Also, many researchers who have focused on choosing basis functions and coupling two adjacent cavities carried out studies on identifying multiple cavities. Morse and Ingard represented the spatial distribution of the radiation from a point source using Green's function theorem to derive the integral equations for coupled cavities surrounded by rigid walls [6]. Dowell et al. developed a comprehensive theoretical model for interior sound fields created by flexible wall motion [14]. They expanded the acoustic pressure and the structural displacement in terms of the normal modes of rigid-walled cavity and in vacuo structural normal modes, respectively. The part connecting two cavities was regarded as a flexible structural member with zero mass and stiffness. Fahy investigated the modal properties of an enclosure coupled to a single Helmholtz resonator [5]. This study reduced the general multimode problem to one of coupling between two modes: the room mode, and the resonator mode. Pan used modal coupling analysis to investigate the free vibration of a coupled panel-cavity system [15,16]. He showed that the interaction strength, expressed as a transfer function, of the uncoupled mode shapes determines the possible energy transfer between two interacting modes. Based on the classical modal coupling method, Sum and Pan proposed an analytical method to improve estimation efficiency of the band-limited response of coupled structural–acoustic systems, particularly in the medium frequency range, where a large number of uncoupled modes are involved [17].

Some researchers defined coupling parameters between an acoustic system and a structural system. Coupling parameters represented the degree of coupling and were expressed as the functions of specific dimensions of each system. Studies showed that changing the parameters could control the dynamic characteristics of the coupled system. Wolf showed that the interaction between the panel and the cavity increases as the cavity becomes shallower (large length/depth ratio) [1]. Hong and Kim defined a non-dimensional coupling parameter, which consisted of a density ratio, an aspect ratio, and a slenderness ratio. They showed that for a relatively shallow cavity the coupling effect increases as the total mass of the acoustic system increases [2,9,10]. Using the structural–acoustic modal coupling coefficients, Kim modified the structure of the panel that contributed the most to vibration in order to reduce interior noise in a half-scaled simplified car [3,4].

Other researchers found control parameters representing an uncoupled acoustic or structural system and used them to change the dynamic characteristics of the coupled structural–acoustic system [18–21]. Kang suggested a noise reduction method for the vehicle passenger compartment that involved tuning the air-gap between the roof and trim-boundary [18]. Lyon studied different control parameters that depended on the frequency range of rectangular enclosures with one flexible wall [19]. Nefske showed the application of a control parameter to reduce interior noise of the automotive passenger compartment [20]. The control parameter considered amplitude-phase indicating panel contribution. Campell predicted and improved vehicle acoustic characteristics using sensitivity analysis [21].

The current study selects new basis functions for three-dimensional (3D) multiple cavities where cavities are connected in series by a neck and derives the governing equations for a coupled system with multiple cavities. The new basis functions will give a new acoustic control parameter, called added length, which affects the

natural frequencies and natural modes of the coupled system. The proposed method with new basis functions gives more accurate results than previous methods for obtaining the modal properties of a coupled structural–acoustic system with multiple cavities where cavities are connected in series by necks. The proposed method is validated by application to a double cavity where two cavities are connected by a neck and structural–acoustic systems with the double cavity.

This work builds on our previous paper [22], but provides a more advanced theoretical approach in terms of assumptions, formulation procedure, and coupling analysis. First, the characteristic equation derived in the previous paper could only be applied to a limited analytical model whose length was much longer than its width and height. However, the characteristic matrix of the governing equation in this paper can be applied to general multiple cavities with no assumptions about length, width and height of cavities. Second, the previous governing equation was derived based on matching boundary conditions at both ends of the acoustic system [23]. This work uses a mode superposition method to obtain an eigenvalue problem. Third, in the previous work only mass–spring systems could be coupled with multiple cavities because only standing waves in the longitudinal direction were considered in the analytical model. This proposed method can work with plates of various boundary conditions because standing waves in all directions (x , y and z axes) are used as basis functions.

This paper is organized in the following way. First, by choosing in vacuo structural modes, rigid-wall acoustic modes, and evanescent acoustic waves as basis functions, theoretical formulation for a general coupled structural–acoustic system is developed. Second, the derived theoretical formulation is applied to a coupled structural–acoustic system with a double cavity. The system includes two rectangular cavities connected by a rectangular neck and blocked by two plates at both ends. Next, the proposed method is validated using finite element analysis (FEA) and compared with the previous method, which had not chosen evanescent waves as basis functions for multiple cavities with necks. The effect of the neck on the modal properties is discussed for four cases. Finally, conclusions are outlined in the last section.

2. Theoretical formulation

2.1. Basic equations

Neglecting damping, the acoustical characteristics of a coupled structural–acoustic system are governed by an inhomogeneous wave equation and the Euler equation expressed by Eqs. (1) and (2), respectively:

$$\nabla^2 \tilde{p}(\vec{r}, t) - \frac{1}{c^2} \frac{\partial^2 \tilde{p}(\vec{r}, t)}{\partial t^2} = -\frac{\partial}{\partial t} \{ \dot{\tilde{m}}(\vec{r}, t) \}, \quad \vec{r} = (x, y, z), \quad (1)$$

$$\nabla \tilde{p}(\vec{r}, t) = -\rho_a \frac{\partial \tilde{u}(\vec{r}, t)}{\partial t}, \quad (2)$$

where $\tilde{p}(\vec{r}, t)$ and $\tilde{u}(\vec{r}, t)$ are the acoustic pressure and the particle velocity at the position vector \vec{r} in the cavity, respectively. c is the speed of sound and ρ_a is the density of the acoustic medium. $\dot{\tilde{m}}(\vec{r}, t)$ is the net influx of the mass per unit time and is composed of the regular mass flow inputs and the effective flow input due to structural motion [9].

The transverse vibration of an undamped thin plate backed by an acoustic system is represented by the fourth-order linear differential equation [24–26]

$$D_E \nabla^4 \tilde{\xi}(\vec{r}_s, t) + \rho_s'' \frac{\partial^2 \tilde{\xi}(\vec{r}_s, t)}{\partial t^2} = {}_s\tilde{p}(\vec{r}_s, t) + \tilde{f}(\vec{r}_s, t), \quad (3)$$

where $\tilde{\xi}(\vec{r}_s, t)$ is the structural displacement at the position vector \vec{r}_s on the plate. ${}_s\tilde{p}(\vec{r}_s, t)$ and $\tilde{f}(\vec{r}_s, t)$ are the acoustic pressure applied to the plate and the external transverse load per unit area, respectively. ρ_s'' is the area density of the plate, and the flexural rigidity of the plate D_E is

$$D_E = \frac{E \cdot t_s^3}{12(1 - \nu^2)}, \quad (4)$$

where E is the Young's modulus of elasticity, t_s the plate thickness and ν Poisson's ratio.

Assuming harmonic motion for the acoustic and structural variables: $\tilde{p}(\vec{r}, t) = p(\vec{r}) \cdot e^{j\omega t}$, $\tilde{u}(\vec{r}, t) = u(\vec{r}) \cdot e^{j\omega t}$, and $\tilde{\xi}(\vec{r}_s, t) = \xi(\vec{r}_s) \cdot e^{j\omega t}$, where ω is the angular frequency and j is the imaginary unit $\sqrt{-1}$, Eqs. (1)–(3) can be translated into Eqs. (5)–(7):

$$\nabla^2 p(\vec{r}) + k^2 p(\vec{r}) = \omega^2 m(\vec{r}), \tag{5}$$

where $k(= \omega/c)$ is the wavenumber:

$$\nabla p(\vec{r}) = -j\omega \rho_a u(\vec{r}), \tag{6}$$

$$D_E \nabla^4 \xi(\vec{r}_s) - \rho_s'' \omega^2 \xi(\vec{r}_s) = {}_s p(\vec{r}_s) + f_s(\vec{r}_s), \tag{7}$$

where ${}_s p(\vec{r}_s)$ consists of internal acoustic pressure and external acoustic pressure. Only internal acoustic pressure is considered in this analysis.

2.2. Base functions for coupling analysis

As shown in Ref. [22], acoustic pressure should be described as the sum of standing waves $\tilde{p}^s(\vec{r}, t)$ and evanescent waves $\tilde{p}^e(\vec{r}, t)$ for multiple cavities with slits or necks:

$$\tilde{p}(\vec{r}, t) = \tilde{p}^s(\vec{r}, t) + \tilde{p}^e(\vec{r}, t). \tag{8}$$

Standing waves $\tilde{p}^s(\vec{r}, t)$ can be expressed as the superposition of rigid-wall acoustic modes $\psi_{d^s}^s$. Evanescent waves $\tilde{p}^e(\vec{r}, t)$ can be expressed as the superposition of a decaying wave $\psi_{d^e}^e$ with a cross-mode, which is a rigid-wall mode in the other two directions perpendicular to the decaying wave:

$$\tilde{p}^s(\vec{r}, t) = p^s(\vec{r}) e^{j\omega t} = \sum_{d^s} A_{d^s} \psi_{d^s}^s(\vec{r}) e^{j\omega t}, \tag{9}$$

$$\tilde{p}^e(\vec{r}, t) = p^e(\vec{r}) e^{j\omega t} = \sum_{d^e} A_{d^e} \psi_{d^e}^e(\vec{r}) e^{j\omega t}, \tag{10}$$

where $\psi_{d^s}^s$ is the d^s th rigid-wall acoustic mode, and $\psi_{d^e}^e$ is the decaying wave with the d^e th cross-mode. They satisfy the homogenous wave Eqs. (11) and (12), respectively:

$$\nabla^2 \psi_{d^s}^s(\vec{r}) + {}_c k_{d^s}^2 \psi_{d^s}^s(\vec{r}) = 0, \tag{11}$$

where ${}_c k_{d^s} = {}_c \omega_{d^s} / c$ and ${}_c \omega_{d^s}$ is the d^s th natural angular frequency:

$$\nabla^2 \psi_{d^e}^e(\vec{r}) + k^2 \psi_{d^e}^e(\vec{r}) = 0. \tag{12}$$

The vibration of the plate in a coupled structural–acoustic system can be expressed as

$$\tilde{\xi}(\vec{r}_s, t) = \xi(\vec{r}_s) e^{j\omega t} = \sum_m B_m \psi_m(\vec{r}_s) e^{j\omega t}, \tag{13}$$

where the in vacuo structural mode of the plate ψ_m satisfies the homogeneous Eq. (14):

$$D_E \nabla^4 \psi_m(\vec{r}_s) - \rho_{ss}'' \omega_m^2 \psi_m(\vec{r}_s) = 0, \tag{14}$$

where ${}_s \omega_m$ is the m th natural angular frequency.

Using basis functions written above, Eqs. (5) and (7) are translated into Eqs. (15) and (16), respectively:

$$\sum_{d^s} A_{d^s} (k^2 - {}_c k_{d^s}^2) \psi_{d^s}^s(\vec{r}) = \omega^2 m(\vec{r}), \tag{15}$$

$$\sum_m B_m \rho_s'' ({}_s \omega_m^2 - \omega^2) \psi_m(\vec{r}_s) = \sum_{d^s} A_{d^s} \psi_{d^s}^s(\vec{r}_s) + f_s(\vec{r}_s). \tag{16}$$

In Eq. (15), $m(\vec{r})$ includes a term created due to evanescent waves in a coupled system with multiple cavities as well as terms representing the regular mass flow inputs and the effect of structural vibration. Therefore, the coupling equations, instead of being expressed by a physical variable, were expressed by rigid-cavity modes,

evanescent waves, in vacuo structural modes, and their coefficients. The coefficients A_{d^s} , B_m and A_{d^e} will be determined by eigenvalue analysis and the velocity continuity condition at the interface between a cavity and a neck.

2.3. Coefficient of an evanescent wave

Evanescent wave in Eq. (8) is considered due to discontinuity in the cross-section at the interface between a cavity and a neck, and its coefficient A_{d^e} is determined by the velocity continuity condition [22]. It is represented as Eq. (17) when the cavity of the cross-sectional area S_i is connected to a neck on its left side ($x = a_i$):

$$\tilde{u}(\vec{r}_{a_i}, t) = \begin{cases} d\tilde{\xi}_n(\vec{r}_{a_i}, t)/dt & \text{only for } S_n, \\ 0 & \text{otherwise,} \end{cases} \quad \vec{r}_{a_i} = (a_i, y, z), \tag{17}$$

where n denotes the neck, $\tilde{\xi}_n(\vec{r}_{a_i}, t)$ is a particle displacement at \vec{r}_{a_i} in the neck, S_n denotes a cross-section of a neck and \vec{r}_{a_i} represents the interface.

Considering Eqs. (8)–(10), Eq. (6) is converted into

$$\sum_{d^s} A_{d^s} \frac{\partial \psi_{d^s}^s(\vec{r}_{a_i})}{\partial x} + \sum_{d^e} A_{d^e} \frac{\partial \psi_{d^e}^e(\vec{r}_{a_i})}{\partial x} = -j\rho_a \omega u(\vec{r}_{a_i}), \tag{18}$$

where the first term on the left-hand side is always zero because the first derivative of the rigid-wall mode $\psi_{d^s}^s$ is zero at the boundary of a cavity. Hence, the coefficient A_{d^e} of the evanescent wave can be determined from Eqs. (10) and (17) by the orthogonality of trigonometric functions:

$$A_{d^e} = -\frac{1}{\alpha_{d^e}} \frac{\rho_a \omega^2 \xi_n \int \psi_{d^e}^e(\vec{r}_{a_i}) dS_n}{\int (\psi_{d^e}^e(\vec{r}_{a_i}))^2 dS_i}, \tag{19}$$

where α_{d^e} describes the decay rate of each evanescent wave. The sign of the decay rate can change depending on the relative position between a cavity and a neck.

3. Theoretical formulation for a coupled structural–acoustic system with a double cavity

As shown in Fig. 1, the coupled system consists of two clamped thin plates and two rectangular cavities connected by a neck with a rectangular cross-section. The neck is located at a point ${}_y g_n$ in the y -direction and ${}_z g_n$ in the z -direction away from the center of a cavity (see Fig. 2). A clamped plate blocked one side of each rectangular cavity and other sides are rigid walls. The cross-sections of the two cavities have the same center. The length l_n of the neck is much shorter than the wavelength of the frequency of interest so that the fluid in the neck can be regarded as a lumped mass element: $k \cdot l_n \ll 1$.

3.1. Governing equations

The governing equations of each cavity and each plate are written as superposition of in vacuo structural modes, rigid-wall acoustic modes, and the net influx of the mass:

$$\sum_{d_1^s} c_1 A_{d_1^s} (k^2 - c_1 k_{d_1^s}^2) c_1 \psi_{d_1^s}^s(\vec{r}) = \omega^2 m_{c_1}(\vec{r}), \tag{20}$$

$$\sum_{m_1} {}_{s_1} B_{m_1} \rho_s'' ({}_{s_1} \omega_{m_1}^2 - \omega^2) {}_{s_1} \psi_{m_1}(\vec{r}_{s_1}) = \sum_{d_1^s} c_1 A_{d_1^s} c_1 \psi_{d_1^s}^s(\vec{r}_{s_1}) + f_{s_1}(\vec{r}_{s_1}), \tag{21}$$

$$\sum_{d_2^s} c_2 A_{d_2^s} (k^2 - c_2 k_{d_2^s}^2) c_2 \psi_{d_2^s}^s(\vec{r}) = \omega^2 m_{c_2}(\vec{r}), \tag{22}$$

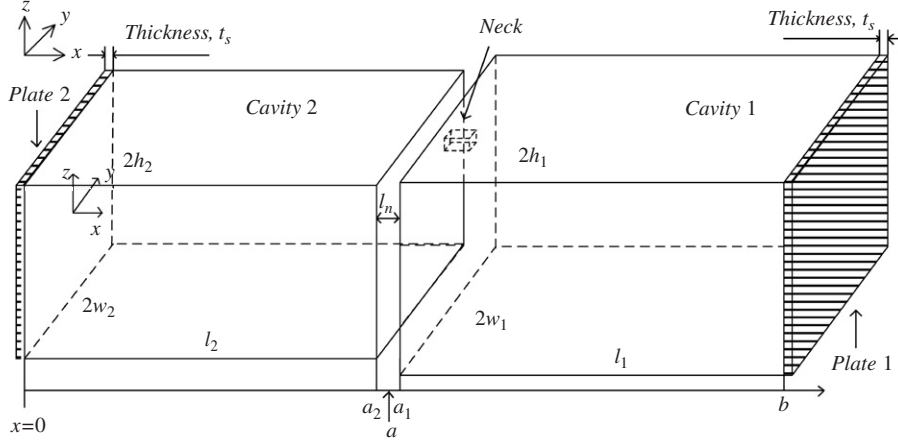


Fig. 1. The three-dimensional coupled structural–acoustic system with the double cavity: two clamped plates blocked both ends of the two cavities connected by a neck and the neck moves vertically on the interface.

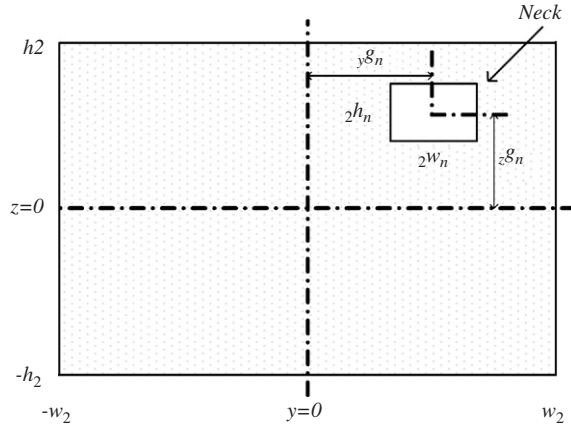


Fig. 2. Cross-section at $x = a$.

$$\sum_{m_2}^{M_2} s_2 B_{m_2} \rho_s'' (s_2 \omega_m^2 - \omega^2) s_2 \psi_{m_2}(\vec{r}_{s_2}) = - \sum_{d_2}^{D_2^s} c_2 A_{d_2} s_2 \psi_{d_2}^s(\vec{r}_{s_2}) + f_{s_2}(\vec{r}_{s_2}), \quad (23)$$

where the subscript c_i and s_j denote the i th cavity and the j th plate, respectively, and $\vec{r}_{s_1} = (b, y, z)$ represents a point on plate 1 and $\vec{r}_{s_2} = (0, y, z)$ represents a point on plate 2. D_i^s and M_j are the total number of acoustic modes and structural modes, respectively.

The equation of motion of the fluid in a neck at $x = a$ becomes

$$\rho_a l_n S_n \frac{d^2 \tilde{\zeta}_n(t)}{dt^2} = \int \tilde{p}_2(\vec{r}_{a_2}, t) dS_n - \int \tilde{p}_1(\vec{r}_{a_1}, t) dS_n, \quad (24)$$

where $\tilde{\zeta}_n(t)$ represents the displacement of the lumped mass in a neck [22].

Considering Eqs. (8)–(10), Eq. (24) is translated into Eq. (25)

$$\rho_a S_n \omega^2 \tilde{\zeta}_n (l_n + \Delta l_1 + \Delta l_2) = \sum_{d_1}^{D_1^s} c_1 A_{d_1} \int c_1 \psi_{d_1}^s(\vec{r}_{a_1}) dS_n - \sum_{d_2}^{D_2^s} c_2 A_{d_2} \int c_2 \psi_{d_2}^s(\vec{r}_{a_2}) dS_n, \quad (25)$$

where each added length Δl_i is represented by Eq. (26):

$$\Delta l_i = (-1)^i \int p_{c_i}^e(\vec{r}_{a_i}) dS_n / (\rho_a S_n \omega^2 \xi_n), \quad (26)$$

where evanescent waves $p_{c_1}^e(\vec{r}_{a_1})$ and $p_{c_2}^e(\vec{r}_{a_2})$ in each rectangular cavity are rewritten as follows:

$$p_{c_1}^e(\vec{r}) = \sum_{m_1^e=0} \sum_{n_1^e=0} c_1 C_{m_1^e n_1^e c_1} \Theta_{m_1^e n_1^e}(y, z) e^{-\alpha_{m_1^e n_1^e} (x-a_1)}, \quad (27)$$

$$p_{c_2}^e(\vec{r}) = \sum_{m_2^e=0} \sum_{n_2^e=0} c_2 C_{m_2^e n_2^e c_2} \Theta_{m_2^e n_2^e}(y, z) e^{\alpha_{m_2^e n_2^e} (x-a_2)}, \quad (28)$$

where two indices (m_i^e and n_i^e) are not zero at the same time, and each cross-mode $c_i \Theta_{m_i^e n_i^e}$ is represented by Eq. (29):

$$c_i \Theta_{m_i^e n_i^e}(\vec{r}) = \cos\left(i k_{m_i^e} (y - w_i)\right) \cos\left(i k_{n_i^e} (z - h_i)\right), \quad (29)$$

where h_i and w_i are the halves of the height and width of each cavity, respectively.

Coefficients $c_i C_{m_i^e n_i^e}$ are calculated by Eq. (19):

$$c_i C_{m_i^e n_i^e} = (-1)^i \frac{\rho_a \omega^2 \xi_n c_i \phi_{m_i^e}(w_i, y g_n) c_i \phi_{n_i^e}(h_i, z g_n)}{\alpha_{m_i^e n_i^e} \varepsilon_{m_i^e n_i^e} h_i w_i}, \quad (30)$$

$$c_i \phi_{m_i^e}(w_i, y g_n) = \int_{y g_n - w_n}^{y g_n + w_n} \cos\left(i k_{m_i^e} (y - w_i)\right) dy, \quad (31)$$

$$c_i \phi_{n_i^e}(h_i, z g_n) = \int_{z g_n - w_n}^{z g_n + h_n} \cos\left(i k_{n_i^e} (z - h_i)\right) dz, \quad (32)$$

where $i k_{m_i^e} = m_i^e \pi / (2w_i)$ and $i k_{n_i^e} = n_i^e \pi / (2h_i)$.

$$\varepsilon_{m_i^e n_i^e} = \begin{cases} 1, & m_i^e \neq 0 \text{ and } n_i^e \neq 0, \\ 2, & m_i^e \neq 0 \text{ and } n_i^e = 0 \text{ or } m_i^e = 0 \text{ and } n_i^e \neq 0, \end{cases} \quad (33)$$

$$\alpha_{m_i^e n_i^e} = \sqrt{\left(\frac{m_i^e \pi}{2w_i}\right)^2 + \left(\frac{n_i^e \pi}{2h_i}\right)^2 - k^2}, \quad (34)$$

$m_{c_i}(\vec{r})$ in Eqs. (20) and (22) is expressed in terms of the structural displacement of the plate blocking each cavity, displacement of the lumped mass in a neck and a regular flow input to each acoustic cavity:

$$m_{c_1}(\vec{r}) = -\rho_a \left(\sum_{m_1}^{M_1} s_1 B_{m_1 s_1} \psi_{m_1} - \zeta_{a_1}(\vec{r}_{a_1}) \text{HF} - 1/(j\omega) \sum_{g_1} q_{g_1} \delta(\vec{r} - \vec{r}_{g_1}) \right), \quad (35)$$

$$m_{c_2}(\vec{r}) = \rho_a \left(\sum_{m_2}^{M_2} s_2 B_{m_2 s_2} \psi_{m_2} - \zeta_{a_2}(\vec{r}_{a_2}) \text{HF} + 1/(j\omega) \sum_{g_2} q_{g_2} \delta(\vec{r} - \vec{r}_{g_2}) \right), \quad (36)$$

where q_{g_i} is the amplitude of the regular mass flow input and $\delta(\vec{r} - \vec{r}_{g_i})$ is Dirac delta function at a point $\vec{r}_{g_i} = (g_i, y, z)$ in cavity i . Also, HF is the product of two Heaviside functions H in the y and z directions. $2w_n$ and $2h_n$ are the width and height of the neck, respectively:

$$\text{HF} = [H\{y - (y g_n - w_n)\} - H\{y - (y g_n + w_n)\}] [H\{z - (z g_n - h_n)\} - H\{z - (z g_n + h_n)\}]. \quad (37)$$

Using the orthogonality of trigonometric functions, Eqs. (20)–(23) are translated into the following equations:

$$c_1 A_{d_1^s} \left(k^2 - c_1 k_{d_1^s}^2 \right) \int \left\{ c_1 \psi_{d_1^s}^s(\vec{r}) \right\}^2 dV_1 = -\omega^2 \rho_a \left(\begin{array}{l} \sum_{m_1}^{M_1} B_{m_1} \int_{s_1} c_1 \psi_{d_1^s}^s(\vec{r}_{s_1})_{s_1} \psi_{m_1}(\vec{r}_{s_1}) dS_1 \\ - \zeta_n \int \text{HF}_{c_1} \psi_{d_1^s}^s(\vec{r}_{a_1}) dS_1 \\ - \sum_{g_1} \int \frac{q_{g_1}}{j\omega} \delta(\vec{r} - \vec{r}_{g_1}) c_1 \psi_{d_1^s}^s(\vec{r}) dV_1 \end{array} \right), \quad (38)$$

$$B_{m_1} \rho_s'' \left(s_1 \omega_{m_1}^2 - \omega^2 \right) \int_{s_1} \psi_{m_1}^2(\vec{r}_{s_1}) dS_1 = \sum_{d_1^s}^{D_1^s} c_1 A_{d_1^s} \int c_1 \psi_{d_1^s}^s(\vec{r}_{s_1})_{s_1} \psi_{m_1}(\vec{r}_{s_1}) dS_1 + \int f_{s_1}(\vec{r}_{s_1})_{s_1} \psi_{m_1}(\vec{r}_{s_1}) dS_1, \quad (39)$$

$$c_2 A_{d_2^s} \left(k^2 - c_2 k_{d_2^s}^2 \right) \int \left\{ c_2 \psi_{d_2^s}^s(\vec{r}) \right\}^2 dV_2 = \omega^2 \rho_a \left(\begin{array}{l} \sum_{m_2}^{M_2} B_{m_2} \int_{s_2} c_2 \psi_{d_2^s}^s(\vec{r}_{s_2})_{s_2} \psi_{m_2}(\vec{r}_{s_2}) dS_2 \\ - \zeta_n \int \text{HF}_{c_2} \psi_{d_2^s}^s(\vec{r}_{a_2}) dS_2 \\ + \sum_{g_2} \int \frac{q_{g_2}}{j\omega} \delta(\vec{r} - \vec{r}_{g_2}) c_2 \psi_{d_2^s}^s(\vec{r}) dV_2 \end{array} \right), \quad (40)$$

$$B_{m_2} \rho_s'' \left(s_2 \omega_{m_2}^2 - \omega^2 \right) \int_{s_2} \psi_{m_2}^2(\vec{r}_{s_2}) dS_2 = - \sum_{d_2^s}^{D_2^s} c_2 A_{d_2^s} \int c_2 \psi_{d_2^s}^s(\vec{r}_{s_2})_{s_2} \psi_{m_2}(\vec{r}_{s_2}) dS_2 + \int f_{s_2}(\vec{r}_{s_2})_{s_2} \psi_{m_2}(\vec{r}_{s_2}) dS_2, \quad (41)$$

Eq. (25) is rewritten as Eq. (42):

$$\zeta_n = 1 / (\rho_a S_n \omega^2 l'_n) \left(\sum_{d_1^s}^{D_1^s} c_1 A_{d_1^s} \int c_1 \psi_{d_1^s}^s(\vec{r}_{a_1}) dS_n - \sum_{d_2^s}^{D_2^s} c_2 A_{d_2^s} \int c_2 \psi_{d_2^s}^s(\vec{r}_{a_2}) dS_n \right), \quad (42)$$

where l'_n is the effective length of a neck, which consists of the neck's real length l_n and total added length $\Delta l_n (= \Delta l_1 + \Delta l_2)$: $l'_n = l_n + \Delta l_1 + \Delta l_2$.

For the convenience of analysis, the following symbols are used:

$$c_i I_{d_i^s} = \int \left\{ c_i \psi_{d_i^s}^s(\vec{r}) \right\}^2 dV_i, \quad s_j I_{m_j} = \int_{s_j} \psi_{m_j}^2(\vec{r}_{s_j}) dS_j, \quad (43a,b)$$

$$c_i J_{d_i^s m_j} = \int c_i \psi_{d_i^s}^s(\vec{r}_{s_j})_{s_j} \psi_{m_j}(\vec{r}_{s_j}) dS_j, \quad (44)$$

$$c_i K_{d_i^s} = \int c_i \psi_{d_i^s}^s(\vec{r}_{a_i}) \text{HF} dS_i, \quad c_i N_{d_i^s} = \int c_i \psi_{d_i^s}^s(\vec{r}_{a_i}) dS_n, \quad (45a,b)$$

$$s_j F_{m_j} = \int f_{m_j}(\vec{r}_{s_j})_{s_j} \psi_{m_j}(\vec{r}_{s_j}) dS_j, \quad q_i Q_{g_i d_i^s} = \int q_{g_i} \delta(\vec{r} - \vec{r}_{g_i}) c_i \psi_{d_i^s}^s(\vec{r}) dV_i. \quad (46a,b)$$

Substituting Eq. (42) into Eqs. (38) and (40), Eqs. (38)–(41) are replaced with Eqs. (47)–(50):

$$c_1 A_{d_1^s} \left(\omega^2 - c_1 \omega_{d_1^s}^2 \right) c_1 I_{d_1^s} + \omega^2 \rho_a c^2 \sum_{m_1}^{M_1} s_1 B_{m_1 c_1} J_{d_1^s m_1} - \frac{c^2}{S_n l'_n} \left(\sum_{d_1^s}^{D_1^s} c_1 A_{d_1^s} c_1 K_{d_1^s c_1} N_{d_1^s} - \sum_{d_2^s}^{D_2^s} c_2 A_{d_2^s} c_1 K_{d_1^s c_2} N_{d_2^s} \right) = -j\omega \rho_a c^2 \sum_{g_1} c_1 Q_{g_1 d_1^s}, \tag{47}$$

$$c_2 A_{d_2^s} \left(\omega^2 - c_2 \omega_{d_2^s}^2 \right) \cdot c_2 I_{d_2^s} - \omega^2 \rho_a c^2 \sum_{m_2}^{M_2} s_2 B_{m_2} \cdot c_2 J_{d_2^s m_2} + \frac{c^2}{S_n \cdot l'_n} \left(\sum_{d_1^s}^{D_1^s} c_1 A_{d_1^s} \cdot c_2 K_{d_2^s} \cdot c_1 N_{d_1^s} - \sum_{d_2^s}^{D_2^s} c_2 A_{d_2^s} \cdot c_2 K_{d_2^s} \cdot c_2 N_{d_2^s} \right) = -j\omega \rho_a c^2 \sum_{g_2} c_2 Q_{g_2 d_2^s}, \tag{48}$$

$$\sum_{d_1^s}^{D_1^s} c_1 A_{d_1^s} c_1 J_{d_1^s m_1} + B_{m_1} \rho_s'' \left(\omega^2 - s_1 \omega_{m_1}^2 \right) s_1 I_{m_1} = -s_1 F_{m_1}, \tag{49}$$

$$- \sum_{d_2^s}^{D_2^s} c_2 A_{d_2^s} c_2 J_{d_2^s m_2} + B_{m_2} \rho_s'' \left(\omega^2 - s_2 \omega_{m_2}^2 \right) s_2 I_{m_2} = -s_2 F_{m_2}, \tag{50}$$

where $c_i J_{d_i^s m_j}$, which is determined by the integral of the cavity mode and the panel mode on the contacting surface, gives information on how the d_i^s th acoustic mode are coupled with the m_j th structural mode of each coupled system. $c_i K_{d_i^s}$ and l'_n include the effect of the neck on the coupled system. While $c_i J_{d_i^s m_j}$ is determined by the similarity of two uncoupled modes, $c_i K_{d_i^s}$ and l'_n depend on the cross-sectional area and the position of the neck. In the verification section, only the effect of the neck’s position will be discussed.

3.2. Matrix formulation

By taking the first D_1^s uncoupled modes of cavity 1, the first D_2^s uncoupled modes of cavity 2, the first M_1 uncoupled modes of plate 1 and the first M_2 uncoupled modes of plate 2, Eqs. (47)–(50) can be written in the following matrix form:

$$[\omega^2 \cdot \mathbf{SMA} - \mathbf{SMB} - \mathbf{SMC}] \cdot \mathbf{X} = \mathbf{F}. \tag{51}$$

The first block matrix **SMA** on the left-hand side of Eq. (51) is the upper triangular matrix represented by Eq. (52), and the second block matrix **SMB** is the lower triangular matrix by Eq. (53):

$$\mathbf{SMA} = \begin{bmatrix} \mathbf{I} & \mathbf{0} & c_1 \mathbf{J}_{d_1^s m_1} & \mathbf{0} \\ \mathbf{0} & \mathbf{I} & \mathbf{0} & -c_2 \mathbf{J}_{d_2^s m_2} \\ \mathbf{0} & \mathbf{0} & \mathbf{I} & \mathbf{0} \\ \mathbf{0} & \mathbf{0} & \mathbf{0} & \mathbf{I} \end{bmatrix}, \tag{52}$$

$$\mathbf{SMB} = \begin{bmatrix} c_1 \mathbf{I}_{d_1^s} & \mathbf{0} & \mathbf{0} & \mathbf{0} \\ \mathbf{0} & c_2 \mathbf{I}_{d_2^s} & \mathbf{0} & \mathbf{0} \\ -c_1 \mathbf{J}'_{d_1^s m_1} & \mathbf{0} & s_1 \mathbf{I}_{m_1} & \mathbf{0} \\ \mathbf{0} & c_2 \mathbf{J}'_{d_2^s m_2} & \mathbf{0} & s_2 \mathbf{I}_{m_2} \end{bmatrix}, \tag{53}$$

where **I** is the identity matrix.

The third block matrix **SMC**, not considered in previous methods, represents the interaction between two cavities and a neck:

$$\mathbf{SMC} = \begin{bmatrix} c_1 \mathbf{KN}_{d_1^s} & c_1 \mathbf{KN}_{d_2^s} & \mathbf{0} & \mathbf{0} \\ c_2 \mathbf{KN}_{d_1^s} & c_2 \mathbf{KN}_{d_2^s} & \mathbf{0} & \mathbf{0} \\ \mathbf{0} & \mathbf{0} & \mathbf{0} & \mathbf{0} \\ \mathbf{0} & \mathbf{0} & \mathbf{0} & \mathbf{0} \end{bmatrix}. \tag{54}$$

Sub-block matrices of the above block matrices are represented by Eqs. (55)–(58):

$$c_i \mathbf{I}_{d_i^s} = \begin{bmatrix} c_i \omega_1^2 & 0 & \cdots & 0 \\ 0 & c_i \omega_2^2 & \vdots & \vdots \\ \vdots & \vdots & \ddots & 0 \\ 0 & \cdots & 0 & c_i \omega_{D_i^s}^2 \end{bmatrix}, \quad s_j \mathbf{I}_{m_j^s} = \begin{bmatrix} s_j \omega_1^2 & 0 & \cdots & 0 \\ 0 & s_j \omega_2^2 & \vdots & \vdots \\ \vdots & \vdots & \ddots & 0 \\ 0 & \cdots & 0 & s_j \omega_{M_j}^2 \end{bmatrix}, \tag{55a,b}$$

$$c_i \mathbf{J}_{d_i^s m_j} = \rho_a c^2 \cdot \begin{bmatrix} \frac{1}{c_i I_1} \{ c_i J_{11} & c_i J_{12} & \cdots & c_i J_{1M_j} \} \\ \frac{1}{c_i I_2} \{ c_i J_{21} & c_i J_{22} & \cdots & c_i J_{2M_j} \} \\ \vdots \\ \frac{1}{c_i I_{D_i^s}} \{ c_i J_{D_i^s 1} & c_i J_{D_i^s 2} & \cdots & c_i J_{D_i^s M_j} \} \end{bmatrix}, \tag{56}$$

$$c_i \mathbf{J}'_{d_i^s m_j} = \frac{1}{\rho_s''} \cdot \begin{bmatrix} \frac{1}{s_j I_1} \{ c_i J_{11} & c_i J_{21} & \cdots & c_i J_{D_i^s 1} \} \\ \frac{1}{s_j I_2} \{ c_i J_{12} & c_i J_{22} & \cdots & c_i J_{D_i^s 2} \} \\ \vdots \\ \frac{1}{s_j I_{M_j}} \{ c_i J_{1M_j} & c_i J_{2M_j} & \cdots & c_i J_{D_i^s M_j} \} \end{bmatrix}, \tag{57}$$

$$c_i \mathbf{KN}_{d_j^s} = \frac{c^2}{S_n l_n'} \begin{bmatrix} \frac{1}{c_i I_1} \{ c_i K_{1c_j} N_1 & c_i K_{1c_j} N_2 & \cdots & c_i K_{1c_j} N_{D_j^s} \} \\ \frac{1}{c_i I_2} \{ c_i K_{2c_j} N_1 & c_i K_{2c_j} N_2 & \cdots & c_i K_{2c_j} N_{D_j^s} \} \\ \vdots \\ \frac{1}{c_i I_{D_j^s}} \{ c_i K_{D_j^s c_j} N_1 & c_i K_{D_j^s c_j} N_2 & \cdots & c_i K_{D_j^s c_j} N_{D_j^s} \} \end{bmatrix}. \tag{58}$$

Therefore, structural–acoustic coupling, mathematically represented by $c_i \mathbf{J}_{d_i^s m_j}$ and $c_i \mathbf{J}'_{d_i^s m_j}$, accounts for the structure vibration which affects the interior acoustic response and the acoustic pressure loading that acts on the panel. $c_i \mathbf{KN}_{d_j^s}$ explains the effect of a neck on the dynamic characteristics of the coupled system.

In Eq. (51), a column vector **X** consists of the coefficients of uncoupled modes:

$$\mathbf{X} = \left\{ c_1 \mathbf{A}_{d_1^s}, c_2 \mathbf{A}_{d_2^s}, s_1 \mathbf{B}_{m_1}, s_2 \mathbf{B}_{m_2} \right\}^T, \tag{59}$$

$$c_i \mathbf{A} d_i^s = \{c_i A_1, c_i A_2, c_i A_3, \dots, c_i A_{D_i^s}\}, \quad (60)$$

$$s_j \mathbf{B} m_j = \{s_j B_1, s_j B_2, s_j B_3, \dots, s_j B_{M_j}\}, \quad (61)$$

where the components of a specific eigenvector represent the participation of the corresponding acoustic mode or structural mode to the coupled mode. Column vector \mathbf{F} is composed of acoustic sources in each cavity and external forces applied to the plates:

$$\mathbf{F} = \left\{ \mathbf{Q}_{g_1 d_1^s}, \mathbf{Q}_{g_2 d_2^s}, s_1 \mathbf{F}_{m_1}, s_2 \mathbf{F}_{m_2} \right\}^T. \quad (62)$$

Either or both of the forcing terms may be present, depending on whether the input excitations such as loudspeaker excitations are applied directly to the structure or the cavity:

$$\mathbf{Q}_{g_i d_i^s} = -j\omega\rho_a c^2 \left\{ \sum_{g_i} \frac{Q_{g_i 1}}{c_i I_1}, \sum_{g_i} \frac{Q_{g_i 2}}{c_i I_2}, \sum_{g_i} \frac{Q_{g_i 3}}{c_i I_3}, \dots, \sum_{g_i} \frac{Q_{g_i D_i^s}}{c_i I_{D_i^s}} \right\}, \quad (63)$$

$$s_j \mathbf{F}_{m_j} = -\frac{1}{\rho_s''} \cdot \left\{ \frac{s_j F_1}{s_j I_1}, \frac{s_j F_2}{s_j I_2}, \frac{s_j F_3}{s_j I_3}, \dots, \frac{s_j F_{M_j}}{s_j I_{M_j}} \right\}. \quad (64)$$

To obtain the eigenvalues and eigenvectors of the coupled system, the external force vector \mathbf{F} is taken equal to zero. Hence, Eq. (51) becomes

$$\omega^2 \cdot \mathbf{SMA} \cdot \mathbf{X} = [\mathbf{SMB} + \mathbf{SMC}] \cdot \mathbf{X}. \quad (65)$$

By a procedure similar to Ref. [9], Eq. (65) is translated into the standard eigenvalue problem:

$$\omega^2 \cdot \mathbf{X} = \mathbf{SMA}^{-1} \cdot [\mathbf{SMB} + \mathbf{SMC}] \cdot \mathbf{X}. \quad (66)$$

Since \mathbf{SMC} has the term of ω , Eq. (66) is not a linear eigenvalue problem. If \mathbf{SMC} were constant, Eq. (66) would be a standard form of the eigenvalue problem whose solution could be easily obtained using commercial mathematical software. Hence, an iteration calculation method must be used to obtain the eigenvalue of this matrix for a predetermined \mathbf{SMC} , and only one eigenvalue can be obtained in the final stage of each iteration calculation. In the first stage of each iteration calculation, an initial eigenvalue is determined from the eigenvalue analysis for Eq. (66) excluding \mathbf{SMC} . In the second stage, a new eigenvalue of Eq. (66) is calculated for \mathbf{SMC} that was predetermined from the initial eigenvalue (ω). If the difference between the new eigenvalue in this stage and the eigenvalue in the previous stage is greater than a specified convergence criterion (0.01 Hz), eigenvalue analysis will be repeated for a new \mathbf{SMC} calculated from the new eigenvalue (ω). This iteration method continues until the difference is less than the convergence criterion. In short, coefficients $A_{d_i^s}$ and B_{m_j} are calculated from the eigenvalue analysis of the characteristic matrix (Eq. (66)) including the predetermined coefficients $c_i C_{m_i^s n_i^s}$ of the evanescent wave.

4. Verification and discussion

The proposed method was validated for a 3D acoustic system and three 3D coupled structural–acoustic systems. The acoustic system consisted of two cavities of the same cross-section and different lengths connected by a neck. The shorter cavity (cavity 2) in the first coupled structural–acoustic system was blocked by a plate at the end only ($x = 0$ in Fig. 1). A clamped plate in the second coupled system was located at the end only ($x = b$ in Fig. 1) of the longer cavity (cavity 1). The third coupled system had two cavities, the ends of which were blocked by plates (see Fig. 1). Using Matlab, the theoretical natural frequencies from the proposed method were compared with those obtained from commercial packages (Ansys 5.5 and Sysnoise 5.5) used for FEA. The effect of the neck's position on natural frequencies was investigated for the four systems. Also, the effect of the plate's position on natural modes and natural frequencies in the three coupled systems was discussed.

To calculate the numerical results for the theoretical models, it was assumed that a neck and a cavity were filled with air, and each clamped plate blocking each cavity had the same thickness of 1 mm and the same

material properties: air density ρ_a of 1.12 kg/m³, sound velocity c of 340 m/s, surface density ρ'_s of 7.8 kg/m², Young’s modulus of elasticity E of 210 G Pa, and Poisson’s ratio ν of 0.3. Cavity 1 was 1 m long, 0.64 m wide and 0.44 m high. The length, width and height of a neck were 0.012, 0.064 0.044 m, respectively. The dimension of cavity 2 is the same as those of cavity 1 except that it has a length of 0.34 m.

In the FEA, enough elements and nodes were used to exactly calculate the natural frequencies. The number of hexahedral element and nodes used in acoustic models was 64,016 and 70,602, respectively. Structural models had 1681 nodes and 1600 shell elements. Nodes in each finite element model were distributed with uniform spacing of 0.016 m in the y -direction and with uniform spacing of 0.011 m in the z -direction. They had uniform spacing of 0.034 in cavity 2 and 1/30 in cavity 1 in the x -direction. A neck connecting two cavities consisted of 16 elements. At the interface surface between the acoustic model and the structural model, acoustic nodes coincide with structural nodes. The maximum frequency at which results could be calculated with reasonable accuracy with the mesh and material properties that were used was 1666 Hz, which was calculated by Sysnoise 5.5 [27].

Table 1
Natural frequencies of the double cavity obtained by the proposed method and those by FEA for three positions of a neck

		yg_n (m)	0.1440 × 0	0.1440 × 1	0.1440 × 2
		zg_n (m)	0.0990 × 0	0.0990 × 1	0.0990 × 2
1	Rigid-body mode	FEA	0.00	0.00	0.00
		Theory (with Δl_n)	0.00	0.00	0.00
		Theory (without Δl_n)	0.00	0.00	0.00
2	x -Axial mode	FEA	46.73	45.61	34.99
		Theory (with Δl_n)	46.85	44.63	34.16
		Theory (without Δl_n)	83.57	74.78	61.72
3	x -Axial mode	FEA	173.66	173.38	171.91
		Theory (with Δl_n)	173.60	173.06	171.69
		Theory (without Δl_n)	185.23	180.14	175.92
4	y -Axial mode	FEA	265.71	265.70	265.67
		Theory (with Δl_n)	265.63	265.63	265.62
		Theory (without Δl_n)	265.62	265.63	265.63
5	y -Axial mode	FEA	265.83	269.12	269.91
		Theory (with Δl_n)	265.63	268.96	269.88
		Theory (without Δl_n)	265.63	275.44	278.37
6	x, y -Tangential mode	FEA	315.54	316.94	317.32
		Theory (with Δl_n)	315.37	316.77	317.19
		Theory (without Δl_n)	315.37	319.59	321.62
7	x -Axial mode	FEA	342.28	342.30	341.54
		Theory (with Δl_n)	341.67	341.62	340.88
		Theory (without Δl_n)	346.69	345.75	343.57
8	z -Axial mode	FEA	386.49	386.47	386.43
		Theory (with Δl_n)	386.36	386.36	386.36
		Theory (without Δl_n)	386.36	386.36	386.36
9	z -Axial mode	FEA	386.59	388.86	389.25
		Theory (with Δl_n)	386.36	388.84	389.29
		Theory (without Δl_n)	386.36	393.91	395.19
10	x, z -Tangential mode	FEA	422.30	423.27	423.38
		Theory (with Δl_n)	422.11	423.15	423.27
		Theory (without Δl_n)	422.11	424.81	425.04

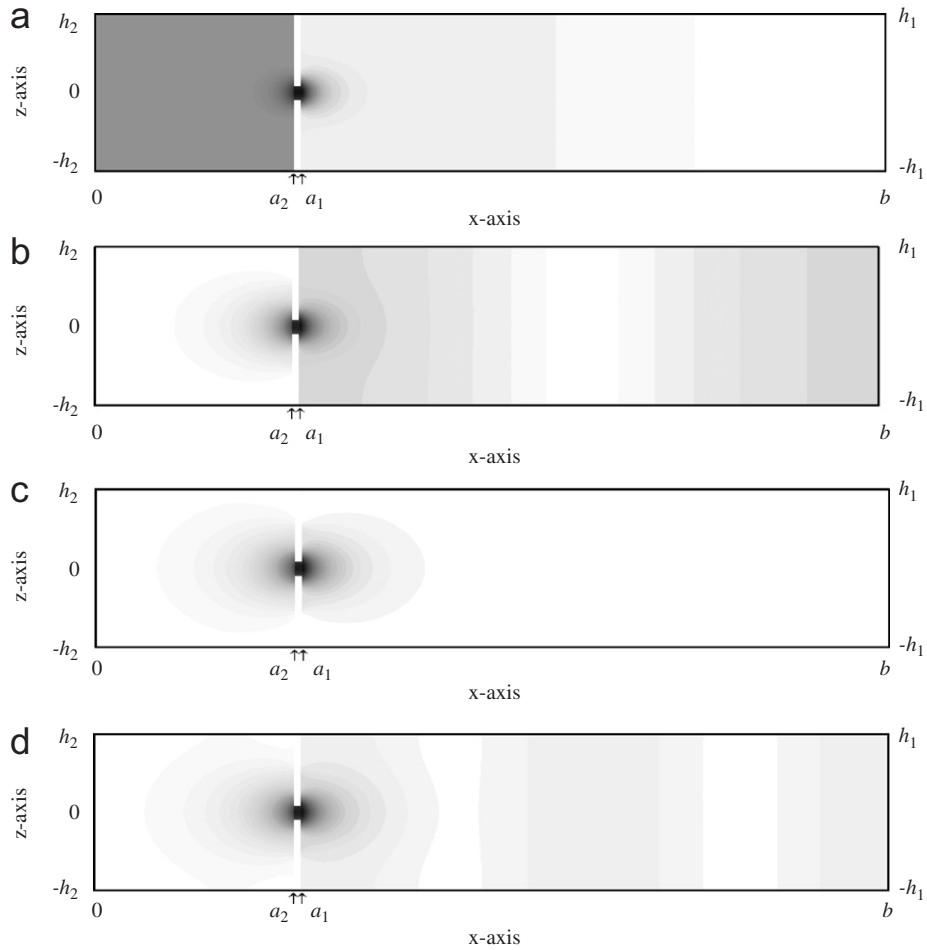


Fig. 3. Acoustic modes of the double cavity with a neck ($y = 0$). Absolute value of acoustic pressure: 0.0 to 1.0. (a) 2nd acoustic mode, (b) 3rd acoustic mode, (c) 5th acoustic mode, (d) 7th acoustic mode.

4.1. Three-dimensional double cavity where two cavities are connected by a neck

Since the geometry of each cavity was simple, basis functions for acoustical coupling analysis were calculated directly from theory. Basis functions consisted of the rigid-wall acoustic modes and natural frequencies. Block matrix ${}_c\mathbf{J}_{\mathbf{d}_i^* \mathbf{m}_j}$ and ${}_c\mathbf{J}_{\mathbf{d}_i^* \mathbf{m}_j}$ of **SMA** and **SMB** in Eq. (65) became $\mathbf{0}$ because this system excluded the structural system. Acoustic natural frequencies of the theoretical model that considered the added length were compared with those obtained by FEA and with those from theoretical model that did not consider the added length. The first ten acoustic modes of each cavity were used to determine the natural frequencies of a double cavity. A neck was placed at three points on the diagonal of the cross-section of cavity 2 (see Fig. 2): the center, the corner, and the mid-point of the center and the corner.

The first ten acoustic natural frequencies that were calculated theoretically and numerically for three positions of the neck are summarized in Table 1. The proposed method gave more accurate results than the previous method, which did not consider evanescent waves for a double cavity with a neck. Natural frequencies of the theoretical model with the added length were close to the results by the FEA, but the theoretical model without the added length gave incorrect results especially for x -axial modes (the 2nd, 3rd, and 7th acoustic modes). The 5th, 6th, 9th and 10th natural frequencies, calculated ignoring the added length, also deviated from those of FEA when a neck was located at the corner. Table 1 also shows that

Table 2
Comparison of natural frequencies obtained by Galerkin’s method and those by FEA for a clamped steel plate

Natural mode	Natural frequency (Hz)		Difference (%)
	Galerkin’s method	FEA	
1	35.48	35.28	0.5
2	56.06	55.63	0.7
3	86.12	85.40	0.8
4	90.51	89.53	1.1
5	105.32	104.09	1.2
6	137.67	135.90	1.3
7	137.94	137.04	0.6
8	162.66	161.02	1.02
9	181.51	179.00	1.40
10	183.44	180.84	1.44
11	197.76	196.86	0.46
12	212.62	211.15	0.70

$$\text{Difference (\%)} = \left| \frac{\text{FEA} - \text{Galerkin's method}}{\text{FEA}} \right| \times 100.$$

Table 3
Natural frequencies of the first coupled structural–acoustic system for three positions of a neck: the double cavity with a neck is blocked by a clamped plate at $x = 0$

		$y g_n$ (m)	0.1440×0	0.1440×1	0.1440×2
		$z g_n$ (m)	0.0990×0	0.0990×1	0.0990×2
1	Rigid body mode	FEA	0.00	0.00	0.00
		Theory (with Δl_n)	0.00	0.00	0.00
		Theory (without Δl_n)	0.00	0.00	0.00
2	Panel-controlled mode	FEA	31.65	31.31	26.90
		Theory (with Δl_n)	31.87	31.10	26.57
		Theory (without Δl_n)	36.03	35.59	34.49
3	Cavity-controlled mode	FEA	54.52	53.79	48.10
		Theory (with Δl_n)	54.41	52.91	47.68
		Theory (without Δl_n)	83.27	76.88	66.08
4	Panel-controlled mode	FEA	55.47	55.48	55.47
		Theory (with Δl_n)	55.78	55.79	55.78
		Theory (without Δl_n)	55.78	55.78	55.77
5	Panel-controlled mode	FEA	85.41	85.41	85.41
		Theory (with Δl_n)	85.85	85.85	85.85
		Theory (without Δl_n)	85.85	85.85	85.85
6	Panel-controlled mode	FEA	90.68	90.67	90.57
		Theory (with Δl_n)	91.33	91.28	91.18
		Theory (without Δl_n)	94.05	92.33	91.54
7	Panel-controlled mode	FEA	104.38	104.38	104.38
		Theory (with Δl_n)	105.15	105.15	105.15
		Theory (without Δl_n)	105.15	105.15	105.15
8	Panel-controlled mode	FEA	136.60	136.60	136.59
		Theory (with Δl_n)	137.55	137.55	137.55
		Theory (without Δl_n)	137.55	137.55	137.55
9	Panel-controlled mode	FEA	136.95	136.95	136.95
		Theory (with Δl_n)	137.70	137.70	137.70
		Theory (without Δl_n)	137.70	137.70	137.70

Table 3 (continued)

		yg_n (m)	0.1440×0	0.1440×1	0.1440×2
		zg_n (m)	0.0990×0	0.0990×1	0.0990×2
10	Panel-controlled mode	FEA	162.09	162.09	162.08
		Theory (with Δl_n)	162.94	162.94	162.93
		Theory (without Δl_n)	162.96	162.96	162.95
11	Cavity-controlled mode	FEA	173.67	173.39	171.91
		Theory (with Δl_n)	173.62	173.07	171.69
		Theory (without Δl_n)	185.31	180.13	175.97
12	Panel-controlled mode	FEA	179.90	179.90	179.90
		Theory (with Δl_n)	181.25	181.25	181.25
		Theory (without Δl_n)	181.25	181.37	181.28
13	Panel-controlled mode	FEA	181.94	181.94	181.94
		Theory (with Δl_n)	183.35	183.35	183.35
		Theory (without Δl_n)	183.35	183.66	183.35
14	Panel-controlled mode	FEA	196.87	196.86	196.86
		Theory (with Δl_n)	197.82	197.81	197.80
		Theory (without Δl_n)	197.93	197.84	197.81
15	Panel-controlled mode	FEA	211.11	211.11	211.11
		Theory (with Δl_n)	212.63	212.62	212.62
		Theory (without Δl_n)	212.66	212.63	212.62
16	Panel-controlled mode	FEA	240.13	240.13	240.13
		Theory (with Δl_n)	242.50	242.50	242.50
		Theory (without Δl_n)	242.50	242.50	242.50
17	Panel-controlled mode	FEA	254.64	254.69	254.70
		Theory (with Δl_n)	256.13	256.22	256.24
		Theory (without Δl_n)	256.13	256.36	256.40
18	Panel-controlled mode	FEA	262.96	262.96	262.96
		Theory (with Δl_n)	264.34	264.34	264.34
		Theory (without Δl_n)	264.34	264.34	264.34
19	Cavity-controlled mode	FEA	264.12	264.74	264.77
		Theory (with Δl_n)	264.50	264.94	264.96
		Theory (without Δl_n)	264.50	265.15	265.16
20	Cavity-controlled mode	FEA	265.74	266.92	267.20
		Theory (with Δl_n)	265.63	267.10	267.52
		Theory (without Δl_n)	265.63	269.32	269.81

the neck's position had an influence on the natural frequencies of the x -axial modes of lower order. The corresponding natural frequencies decreased as the neck approached the corner. As the neck moved from the center to the corner, the number of cross-modes an evanescent wave could have increased, thus increasing the effective length of the neck for x -axial acoustic modes [22]. Fig. 3 displays four acoustic modes of low order, where acoustic pressure distribution around the neck was complicated due to evanescent waves.

These results suggest two facts that should be considered in characterizing modal properties of a double cavity with a neck. First, evanescent waves should be included in the formulation procedure for calculating natural frequencies and their natural modes. Consideration of evanescent waves near the interface reduced the amount of inevitable errors in the mode superposition method for a double cavity. Second, the evanescent wave created due to a neck strongly affected the lower-order longitudinal modes and their natural frequencies, but had less of an effect on the other modes.

4.2. Three coupled structural–acoustic systems: a double cavity blocked by a plate, selectively

Twenty structural modes of a clamped plate and 20 acoustic modes of each cavity obtained from theory were used in the analytical approach for three coupled systems. Table 2 shows the comparison of the natural frequencies of a clamped plate, calculated from the Galerkin’s method, and those calculated by FEA. Coupled natural modes obtained from the proposed method are classified as cavity-controlled modes, where most of the energy is stored in the cavity sound field, and panel-controlled modes, where most of the energy is stored as structural vibration energy [16].

Table 3 shows the first twenty coupled natural frequencies calculated by the proposed method for the first coupled system, where a plate was placed only at $x = 0$. Also, the coupled natural frequencies were compared with those of an analytical model that did not consider the added lengths for the three different positions of the neck. Cavity-controlled modes (the 3rd and 11th coupled modes) and a panel-controlled mode (the 2nd coupled mode) that interacted strongly with the rigid-wall acoustic mode were strongly affected in the lower

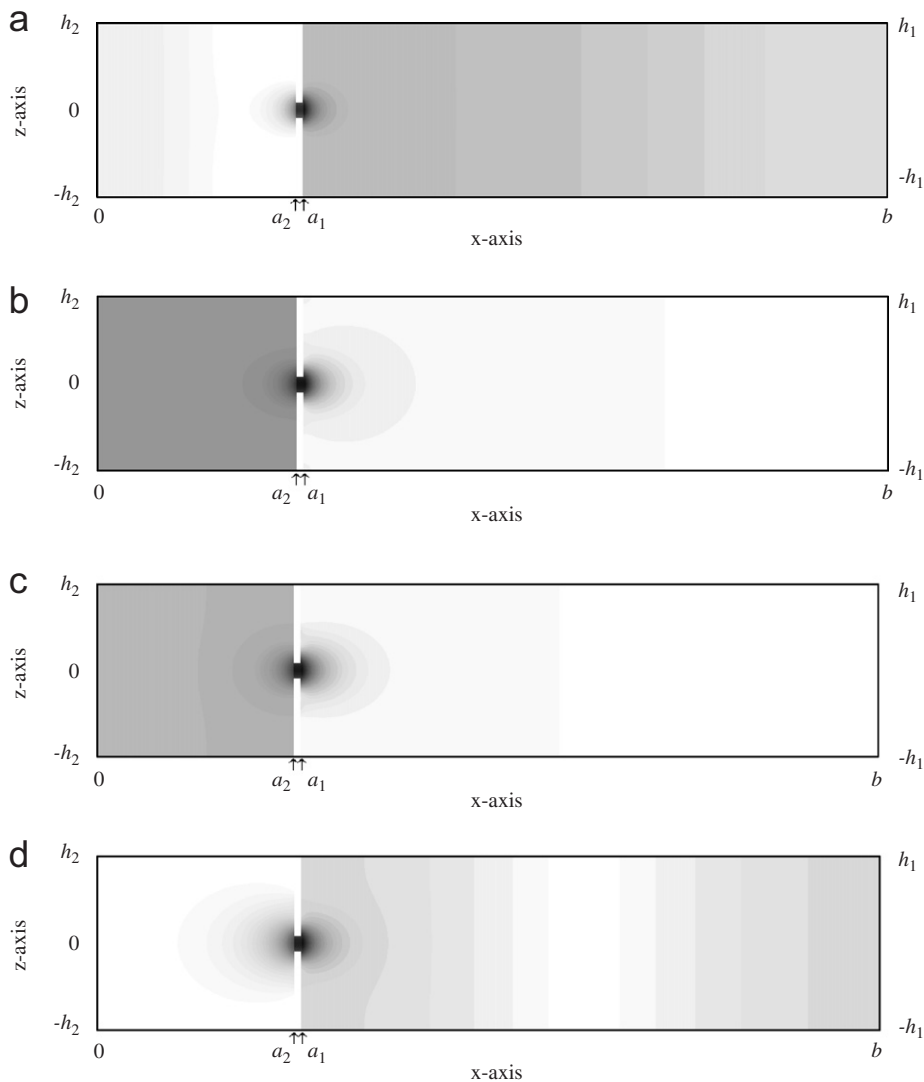


Fig. 4. Acoustic pressure distribution of natural modes of the first coupled system ($y = 0$): the double cavity with a neck is blocked by a clamped plate at $x = 0$. Absolute value of acoustic pressure: $\frac{\text{color}}{1.0}$. (a) 2nd acoustic mode, (b) 3rd acoustic mode, (c) 6th acoustic mode, (d) 11th acoustic mode.

frequency range by the neck's position, but the other coupled modes were not. Fig. 4 represents the acoustic pressure distribution of four coupled natural modes at the surface at $y = 0$. All of the modes had acoustic pressure distribution in the x -axial direction. The associated coupled natural frequencies decreased as the neck moved from the center to the corner. For the 2nd, 3rd, 6th and 11th coupled modes, the analytical model that included added lengths predicted more exact frequencies than the analytical model without the added lengths.

Coupled natural frequencies for a double cavity blocked by a plate at $x = b$ are summarized in Table 4. The variation trend of the coupled natural frequencies with a neck's position was similar to that of the first coupled system. The accuracy of the values was verified by results obtained from FEA for the 2nd, 3rd, 6th and 11th coupled modes. Fig. 5 shows the acoustic pressure distribution of four coupled natural modes on the surface at $y = 0$.

The only difference between Tables 3 and 4 is the degree of coupling, which was determined by three factors: the closeness in natural frequencies between the rigid-wall acoustic mode and the in vacuo structure mode;

Table 4

Natural frequencies of the second coupled structural–acoustic system for three positions of a neck: the double cavity with a neck is blocked by a clamped plate at $x = b$

		$y g_n$ (m)	0.1440×0	0.1440×1	0.1440×2
		$z g_n$ (m)	0.0990×0	0.0990×1	0.0990×2
1	Rigid body mode	FEA	0.00	0.00	0.00
		Theory (with Δl_n)	0.00	0.00	0.00
		Theory (without Δl_n)	0.00	0.00	0.00
2	Panel-controlled mode	FEA	35.77	35.65	32.24
		Theory (with Δl_n)	35.97	35.68	31.82
		Theory (without Δl_n)	36.90	36.84	36.67
3	Cavity-controlled mode	FEA	48.32	47.33	40.15
		Theory (with Δl_n)	48.38	46.28	39.88
		Theory (without Δl_n)	83.58	75.27	62.51
4	Panel-controlled mode	FEA	55.49	55.49	55.49
		Theory (with Δl_n)	55.85	55.85	55.85
		Theory (without Δl_n)	55.86	55.85	55.85
5	Panel-controlled mode	FEA	85.40	85.40	85.40
		Theory (with Δl_n)	85.99	85.99	85.99
		Theory (without Δl_n)	85.99	85.99	85.99
6	Panel-controlled mode	FEA	89.95	89.94	89.92
		Theory (with Δl_n)	90.57	90.57	90.54
		Theory (without Δl_n)	91.29	90.82	90.64
7	Panel-controlled mode	FEA	104.40	104.40	104.40
		Theory (with Δl_n)	105.24	105.24	105.24
		Theory (without Δl_n)	105.24	105.24	105.24
8	Panel-controlled mode	FEA	136.57	136.57	136.57
		Theory (with Δl_n)	137.63	137.63	137.63
		Theory (without Δl_n)	137.63	137.63	137.63
9	Panel-controlled mode	FEA	136.98	136.98	136.98
		Theory (with Δl_n)	137.76	137.76	137.76
		Theory (without Δl_n)	137.76	137.76	137.76
10	Panel-controlled mode	FEA	160.49	160.47	160.31
		Theory (with Δl_n)	161.37	161.32	161.16
		Theory (without Δl_n)	162.09	161.88	161.60
11	Cavity-controlled mode	FEA	176.11	175.87	174.60
		Theory (with Δl_n)	176.12	175.64	174.47
		Theory (without Δl_n)	186.56	181.92	178.13

Table 4 (continued)

		yg_n (m)	0.1440×0	0.1440×1	0.1440×2
		zg_n (m)	0.0990×0	0.0990×1	0.0990×2
12	Panel-controlled mode	FEA	179.94	179.94	179.94
		Theory (with Δl_n)	181.32	181.32	181.32
		Theory (without Δl_n)	181.32	181.32	181.32
13	Panel-controlled mode	FEA	181.95	181.95	181.95
		Theory (with Δl_n)	183.39	183.39	183.39
		Theory (without Δl_n)	183.38	183.39	183.39
14	Panel-controlled mode	FEA	197.14	197.14	197.12
		Theory (with Δl_n)	198.12	198.12	198.10
		Theory (without Δl_n)	198.43	198.24	198.15
15	Panel-controlled mode	FEA	211.16	211.16	211.16
		Theory (with Δl_n)	212.72	212.72	212.71
		Theory (without Δl_n)	212.76	212.74	212.72
16	Panel-controlled mode	FEA	240.13	240.13	240.13
		Theory (with Δl_n)	242.56	242.56	242.56
		Theory (without Δl_n)	242.56	242.56	242.56
17	Panel-controlled mode	FEA	254.80	254.81	254.81
		Theory (with Δl_n)	256.49	256.50	256.50
		Theory (without Δl_n)	256.49	256.51	256.52
18	Panel-controlled mode	FEA	262.98	262.98	262.98
		Theory (with Δl_n)	264.51	264.51	264.51
		Theory (without Δl_n)	264.51	264.51	264.51
19	Cavity-controlled mode	FEA	264.87	264.97	264.96
		Theory (with Δl_n)	265.07	265.16	265.16
		Theory (without Δl_n)	265.07	265.18	265.18
20	Cavity-controlled mode	FEA	265.82	268.24	268.59
		Theory (with Δl_n)	264.62	268.43	269.06
		Theory (without Δl_n)	265.63	270.58	270.73

their mode shapes; and the plate’s position in each coupled system. The 2nd acoustic natural frequency was very close to the 1st structural natural frequency of the clamped plate in two coupled systems. However, the 1st coupled system had stronger coupling than the 2nd coupled system because the acoustic mode (x -axial mode) had higher acoustic pressure in cavity 2 than in cavity 1: the anti-nodal surface is placed near $x = 0$; and the nodal surface near $x = b$ (see Fig. 3(a)). Hence, the difference between the associated coupled frequency and the uncoupled natural frequency was larger for the 1st coupled system than for the 2nd coupled system. On the contrary, the acoustic pressure in the 3rd acoustic mode (x -axial mode) was higher in cavity 1 than in cavity 2 (see Fig. 3(b)). Therefore, the 2nd coupled system had stronger coupling than the 1st coupled system for the 11th coupled mode.

Table 5 compares the natural frequencies of the 3rd coupled system, where plates were clamped at both ends, calculated by the proposed method with those calculated by FEA and those calculated using the analytical model ignoring the added length. The 2nd, 4th and 19th coupled natural frequencies decreased as the neck approached the corner from the center. Investigating the acoustic pressure distribution and structural displacement for each coupled mode revealed that the 4th and 19th modes were cavity-controlled modes and the 2nd coupled mode was a panel-controlled mode. The 2nd and 3rd coupled modes all were panel-controlled modes, but they had different relative displacements between two plates. Since the two plates moved in-phase in the 2nd coupled mode, the net volume displacement by structural vibration in the acoustic field was very small. Hence, the neck’s position had a little effect on the natural frequency. However, the effect of structural vibration on the acoustic field was strong in the 3rd coupled mode, where the two plates moved out-of-phase.

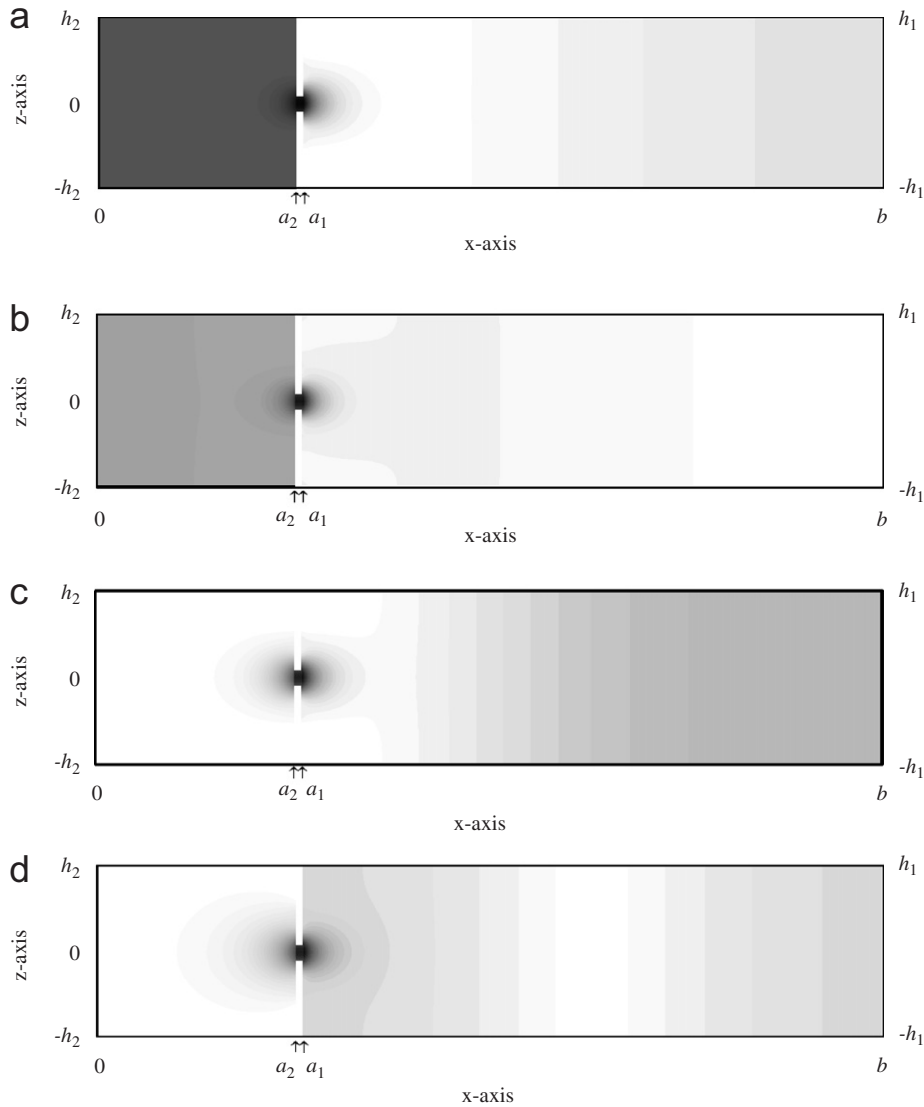


Fig. 5. Acoustic pressure distribution of natural modes of the second coupled system ($y = 0$): the double cavity with a neck is blocked by a clamped plate at $x = b$. Absolute value of acoustic pressure: 0.0 to 1.0. (a) 2nd acoustic mode, (b) 3rd acoustic mode, (c) 6th acoustic mode, (d) 11th acoustic mode.

Results of the analytical model that ignored evanescent waves were different from those found through FEA. The difference was especially pronounced for cavity-controlled modes and panel-controlled modes with strong coupling: the 2nd, 3rd, 4th, 10th and 19th coupled natural modes. Fig. 6 shows the acoustic pressure distribution of four coupled natural modes on the surface at $y = 0$. In coupled modes related to the x -axial acoustic modes, the existence of a neck created a local acoustic field around the neck, and the effect of the neck decreased with distance from the neck in the x -axis. However, oblique modes and tangential modes were hardly affected by the motion of a neck.

Although the proposed method was applied to a double cavity, it can be applied to the coupled structural–acoustic system with multiple cavities with necks. The same procedure that was applied to a double cavity can be used if $c_i \mathbf{KN}_i$ is modified properly in each block matrix of Eq. (54). Also, although the new basis function considered in this paper represented only the evanescent wave decaying in the x -direction with a set of cross-modes in the $y-z$ planes, it can describe the effect of the decay waves with a set of cross-modes in the all

Table 5

Natural frequencies of the third coupled structural–acoustic system for three positions of a neck: the double cavity with a neck is blocked by two clamped plates at $x = 0$ and b

	yg_n (m)		0.1440×0	0.1440×1	0.1440×2
	zg_n (m)		0.0990×0	0.0990×1	0.0990×2
1	Rigid-body mode	FEA	0.00	0.00	0.00
		Theory (with Δl_n)	0.00	0.00	0.00
		Theory (without Δl_n)	0.00	0.00	0.00
2	Panel-controlled mode	FEA	29.93	29.64	25.70
		Theory (with Δl_n)	30.21	29.53	25.45
		Theory (without Δl_n)	33.90	33.51	32.55
3	Panel-controlled mode	FEA	38.52	38.50	38.26
		Theory (with Δl_n)	38.62	38.57	38.35
		Theory (without Δl_n)	39.03	38.96	38.82
4	Cavity-controlled mode	FEA	55.02	54.26	48.39
		Theory (with Δl_n)	54.88	53.35	47.93
		Theory (without Δl_n)	83.29	77.21	66.55
5	Panel-controlled mode	FEA	55.47	55.49	55.47
		Theory (with Δl_n)	55.78	55.79	55.78
		Theory (without Δl_n)	55.78	55.78	55.77
6	Panel-controlled mode	FEA	55.49	55.49	55.49
		Theory (with Δl_n)	55.85	55.85	55.85
		Theory (without Δl_n)	55.85	55.85	55.85
7	Panel-controlled mode	FEA	85.40	85.40	85.41
		Theory (with Δl_n)	85.85	85.85	85.85
		Theory (without Δl_n)	85.85	85.85	85.85
8	Panel-controlled mode	FEA	85.41	85.41	85.41
		Theory (with Δl_n)	85.99	85.99	85.99
		Theory (without Δl_n)	85.99	85.99	85.99
9	Panel-controlled mode	FEA	89.93	89.93	89.92
		Theory (with Δl_n)	90.56	90.55	90.54
		Theory (without Δl_n)	90.61	90.61	90.59
10	Panel-controlled mode	FEA	90.70	90.68	90.58
		Theory (with Δl_n)	91.35	91.29	91.18
		Theory (without Δl_n)	94.62	92.58	91.61
11	Panel-controlled mode	FEA	104.38	104.38	104.38
		Theory (with Δl_n)	105.15	105.15	105.15
		Theory (without Δl_n)	105.15	105.15	105.15
12	Panel-controlled mode	FEA	104.40	104.40	104.40
		Theory (with Δl_n)	105.24	105.24	105.24
		Theory (without Δl_n)	105.24	105.24	105.24
13	Panel-controlled mode	FEA	136.57	136.57	136.57
		Theory (with Δl_n)	137.55	137.55	137.55
		Theory (without Δl_n)	137.55	137.55	137.55
14	Panel-controlled mode	FEA	136.60	136.60	136.59
		Theory (with Δl_n)	137.63	137.63	137.63
		Theory (without Δl_n)	137.63	137.63	137.63
15	Panel-controlled mode	FEA	136.95	136.95	136.95
		Theory (with Δl_n)	137.70	137.70	137.70
		Theory (without Δl_n)	137.70	137.70	137.71

Table 5 (continued)

	yg_n (m)		0.1440×0	0.1440×1	0.1440×2
	zg_n (m)		0.0990×0	0.0990×1	0.0990×2
16	Panel-controlled mode	FEA	136.98	136.98	136.98
		Theory (with ΔI_n)	137.76	137.76	137.76
		Theory (without ΔI_n)	137.76	137.76	137.76
17	Panel-controlled mode	FEA	160.49	160.46	160.31
		Theory (with ΔI_n)	161.37	161.32	161.16
		Theory (without ΔI_n)	162.02	161.83	161.58
18	Panel-controlled mode	FEA	162.10	162.10	162.08
		Theory (with ΔI_n)	162.95	162.95	162.94
		Theory (without ΔI_n)	163.05	163.02	162.99
19	Cavity-controlled mode	FEA	176.17	175.92	174.64
		Theory (with ΔI_n)	176.13	175.65	174.48
		Theory (without ΔI_n)	186.62	182.13	178.15
20	Panel-controlled mode	FEA	179.90	179.90	179.90
		Theory (with ΔI_n)	181.25	181.25	181.25
		Theory (without ΔI_n)	181.25	181.13	181.29
21	Panel-controlled mode	FEA	179.94	179.94	179.94
		Theory (with ΔI_n)	181.32	181.32	181.32
		Theory (without ΔI_n)	181.32	181.32	182.32
22	Panel-controlled mode	FEA	181.94	181.94	181.94
		Theory (with ΔI_n)	183.35	183.35	183.35
		Theory (without ΔI_n)	183.35	183.35	183.35
23	Panel-controlled mode	FEA	181.95	181.95	181.95
		Theory (with ΔI_n)	183.39	183.39	183.39
		Theory (without ΔI_n)	183.39	183.39	183.39
24	Panel-controlled mode	FEA	196.86	196.86	196.86
		Theory (with ΔI_n)	197.81	197.81	197.80
		Theory (without ΔI_n)	197.85	197.83	197.81
25	Panel-controlled mode	FEA	197.15	197.14	197.12
		Theory (with ΔI_n)	198.13	198.12	198.10
		Theory (without ΔI_n)	198.51	198.26	198.16
26	Panel-controlled mode	FEA	211.11	211.11	211.11
		Theory (with ΔI_n)	212.63	212.62	212.62
		Theory (without ΔI_n)	212.64	212.63	212.62
27	Panel-controlled mode	FEA	211.16	211.16	211.16
		Theory (with ΔI_n)	212.72	212.72	212.71
		Theory (without ΔI_n)	212.78	212.74	212.73
28	Panel-controlled mode	FEA	240.13	240.13	240.13
		Theory (with ΔI_n)	242.50	242.50	242.50
		Theory (without ΔI_n)	242.50	242.50	242.50
29	Panel-controlled mode	FEA	240.14	240.14	240.14
		Theory (with ΔI_n)	242.56	242.56	242.56
		Theory (without ΔI_n)	242.56	242.56	242.56
30	Panel-controlled mode	FEA	254.64	254.69	254.70
		Theory (with ΔI_n)	256.13	256.22	256.24
		Theory (without ΔI_n)	256.13	256.34	256.36
31	Panel-controlled mode	FEA	254.81	254.81	254.81
		Theory (with ΔI_n)	256.49	256.50	256.51
		Theory (without ΔI_n)	256.49	256.54	256.56

Table 5 (continued)

	yg_n (m)		0.1440×0	0.1440×1	0.1440×2
	zg_n (m)		0.0990×0	0.0990×1	0.0990×2
32	Panel-controlled mode	FEA	262.96	262.96	262.96
		Theory (with Δl_n)	264.34	264.34	264.34
		Theory (without Δl_n)	264.34	264.34	264.34
33	Panel-controlled mode	FEA	262.98	262.98	262.98
		Theory (with Δl_n)	264.50	264.51	264.51
		Theory (without Δl_n)	264.50	264.51	264.51
34	Cavity-controlled mode	FEA	264.18	264.57	264.56
		Theory (with Δl_n)	264.51	264.82	264.83
		Theory (without Δl_n)	264.51	264.88	264.88
35	Cavity-controlled mode	FEA	264.90	266.01	266.26
		Theory (with Δl_n)	265.07	266.50	266.87
		Theory (without Δl_n)	265.07	268.35	268.74
36	Panel-controlled mode	FEA	270.04	270.30	270.34
		Theory (with Δl_n)	271.42	271.64	271.69
		Theory (without Δl_n)	271.42	271.89	271.95
37	Panel-controlled mode	FEA	272.42	273.93	274.41
		Theory (with Δl_n)	273.81	275.08	275.55
		Theory (without Δl_n)	273.81	279.40	281.86
38	Panel-controlled mode	FEA	281.20	281.20	281.20
		Theory (with Δl_n)	283.39	283.39	283.39
		Theory (without Δl_n)	283.39	283.39	283.39
39	Panel-controlled mode	FEA	281.22	281.22	281.22
		Theory (with Δl_n)	283.48	283.48	283.48
		Theory (without Δl_n)	283.48	283.48	283.48
40	Panel-controlled mode	FEA	310.94	310.94	310.94
		Theory (with Δl_n)	313.82	313.82	313.82
		Theory (without Δl_n)	313.83	313.83	313.82

direction as proved in Eq. (10). As similar to Eqs. (27) and (28), each evanescent wave is expressed by multiplication of cross-mode terms and a decay wave term in each direction:

$$p^e(x, y, z) = \sum_{m_1} C_{m_1} \Theta_{m_1}(y, z)e^{-\alpha_1 x} + \sum_{m_2} C_{m_2} \Theta_{m_2}(z, x)e^{-\alpha_2 y} + \sum_{m_3} C_{m_3} \Theta_{m_3}(x, y)e^{-\alpha_3 z}. \tag{67}$$

5. Conclusions

In this paper, an improved mode superposition method applicable to 3D multiple cavities where cavities were connected in series by necks was proposed. This method increased calculation accuracy of the natural frequencies and that of acoustic pressure distribution of natural modes. In the theoretical formulation, evanescent waves as well as standing waves were used as the basis functions for each cavity to exactly describe the effect of a neck on the modal properties of an acoustic system. The evanescent waves were converted into the added length term (or matrix component) in the characteristic matrix. The added length changed with a neck’s position in the interface between two cavities. The number of participating cross-modes varied with the neck’s position [22]. The existence of the neck strongly affected the longitudinal acoustic mode in the *x*-axis direction.

For multiple cavities where cavities are connected in series by necks and a structural–acoustic system with the multiple cavities, our proposed method is superior in terms of three aspects to the previous mode

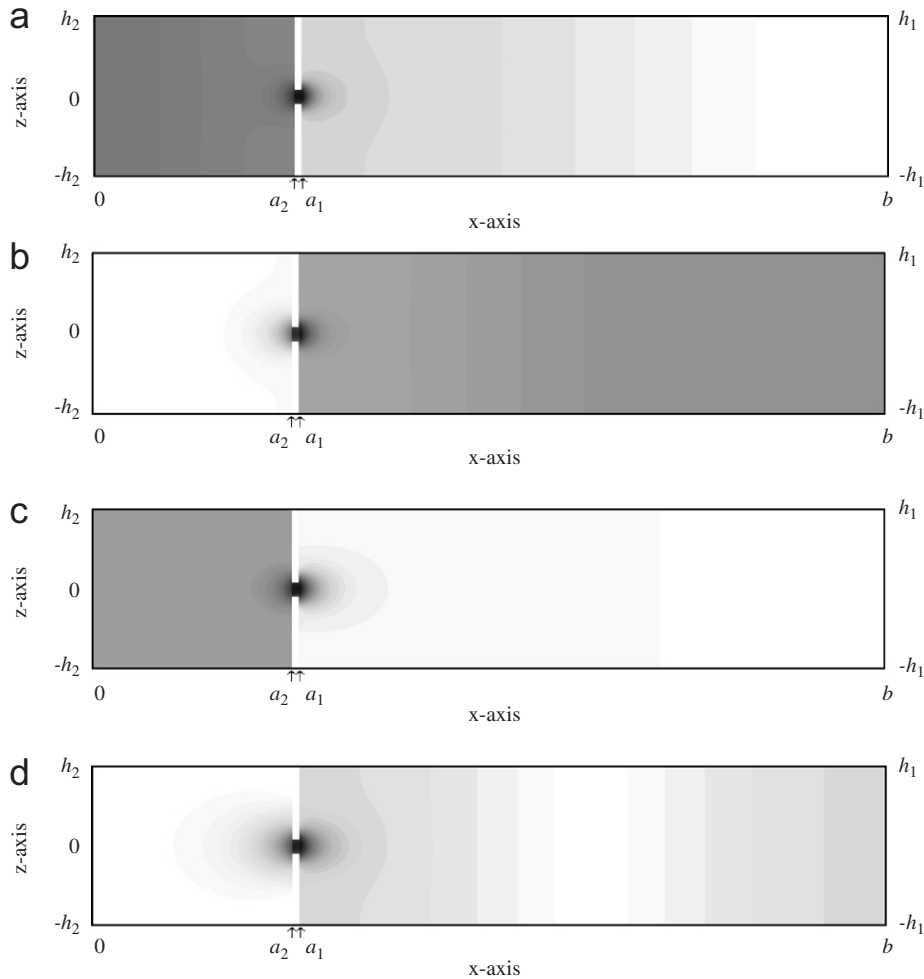


Fig. 6. Acoustic pressure distribution of natural modes of the third coupled system ($y = 0$): the double cavity with a neck is blocked by two clamped plates at $x = 0$ and b . Absolute value of acoustic pressure: . (a) 2nd acoustic mode, (b) 3rd acoustic mode, (c) 4th acoustic mode, (d) 19th acoustic mode.

superposition method, which did not include evanescent wave as a basis function. The three aspects are accuracy of calculated natural frequencies, physical explanation for a neck's effect on natural frequencies and acoustic pressure distribution around a neck. First, comparison of the theoretical results and the FEA results for a double cavity supported the validity of the proposed method (Tables 1–4). Also, the results showed that the neck's position could be changed to control the modal properties of the cavity-controlled mode, which showed acoustic pressure distribution in the longitudinal direction, and those of the panel-controlled mode, which interacted strongly with the cavity mode. Second, the added length, which was converted from evanescent waves, could explain the effect of a neck's position on natural frequencies. The associated natural frequencies decreased because the added length increased as the neck approached the corner from the center. Finally, consideration of evanescent waves enabled the description of the acoustic pressure distribution around a neck based on a theoretical approach.

The proposed method should be used to obtain the modal properties of multiple cavities where cavities are connected by necks and the coupled structural–acoustic system with the multiple cavities. Also, a coupled structural–acoustic system with multiple cavities, which has desirable dynamic characteristics, can be obtained by adjusting the neck's position and the plate position.

Acknowledgments

This work was supported by the Brain Korea 21 project in 2003.

References

- [1] J.A. Wolf Jr., Modal synthesis for combined structural–acoustic systems, *AIAA Journal* 15 (1977) 734–745.
- [2] K.L. Hong, J. Kim, Analysis of free vibration of structural–acoustic coupled systems—part II: two and three dimensional examples, *Journal of Sound and Vibration* 188 (4) (1995) 577–600.
- [3] S.H. Kim, J.M. Lee, A practical method for noise reduction in a vehicle passenger compartment, *ASME/Journal of Vibration and Acoustics* 120 (1998) 199–205.
- [4] S.H. Kim, J.M. Lee, M.H. Sung, Structural–acoustic modal coupling analysis and application to noise reduction in a vehicle passenger compartment, *Journal of Sound and Vibration* 225 (5) (1999) 989–999.
- [5] F.J. Fahy, C. Schofield, A note on the interaction between a Helmholtz resonator and an acoustic mode of an enclosure, *Journal of Sound and Vibration* 72 (3) (1980) 365–378.
- [6] P.M. Morse, K.U. Ingard, *Theoretical Acoustics*, McGraw-Hill Book Company, New York, 1968.
- [7] Z. Ma, I. Hagiwara, Improved mode-superposition technique for modal frequency response analysis of coupled acoustic–structural systems, *AIAA Journal* 29 (10) (1990) 1720–1726.
- [8] J. Luo, H.C. Gea, Modal sensitivity analysis of coupled acoustic–structural systems, *ASME/Journal of Vibration and Acoustics* 119 (1997) 545–550.
- [9] K.L. Hong, J. Kim, Analysis of free vibration of structural–acoustic coupled systems—part I: development and verification of the procedure, *Journal of Sound and Vibration* 188 (4) (1995) 561–575.
- [10] K.L. Hong, J. Kim, New analysis method for general acoustic–structural coupled systems, *Journal of Sound and Vibration* 192 (2) (1996) 465–480.
- [11] S.M. Sung, D.J. Nefske, A coupled structural–acoustic finite element model for vehicle interior noise analysis, *ASME/Journal of Vibration, Acoustics, Stress, and Reliability in Design* 106 (1984) 314–318.
- [12] L.I. Slepyan, S.V. Sorokin, Analysis of structural–acoustic coupling problems by a two-level boundary integral method—part I: a general formulation and test problems, *Journal of Sound and Vibration* 184 (2) (1995) 195–211.
- [13] J.T. Chen, M.H. Chang, K.H. Chen, I.L. Chen, Boundary collocation method for acoustic eigenanalysis of three-dimensional cavities using radial basis function, *Computational Mechanics* 29 (2002) 392–408.
- [14] E.H. Dowell, G.F. Gorman, D.A. Smith, Acoustoelasticity: general theory, acoustic natural modes and forced response to sinusoidal excitation, including comparisons with experiment, *Journal of Sound and Vibration* 52 (4) (1977) 519–542.
- [15] J. Pan, D.A. Bies, The effect of fluid–structural coupling on sound waves in an enclosure—experimental part, *Journal of the Acoustical Society of America* 87 (2) (1990) 708–717.
- [16] J. Pan, D.A. Bies, The effect of fluid–structural coupling on sound waves in an enclosure—theoretical part, *Journal of the Acoustical Society of America* 87 (2) (1990) 691–707.
- [17] K.S. Sum, J. Pan, An analytical model for bandlimited response of acoustic–structural coupled systems. I. Direct sound field excitation, *Journal of the Acoustical Society of America* 103 (2) (1998) 911–923.
- [18] S.W. Kang, J.M. Lee, S.H. Kim, Structural–acoustic coupling analysis of the vehicle passenger compartment with the roof, air-gap, and trim boundary, *ASME/Journal of Vibration and Acoustics* 122 (2000) 196–202.
- [19] R.H. Lyon, Noise reduction of rectangular enclosures with one flexible wall, *Journal of the Acoustical Society of America* 35 (11) (1963) 1791–1797.
- [20] D.J. Nefske, J.A. Wolf Jr., L.J. Howell, Structural–acoustic finite element analysis of the automobile passenger compartment: a review of current practice, *Journal of Sound and Vibration* 80 (2) (1982) 247–266.
- [21] B. Campell, M. Abrishman, W. Stokes, Structural–acoustic analysis for the prediction of vehicle body acoustic sensitivities, *SAE* 931327 (1993) 507–516.
- [22] J.W. Lee, J.M. Lee, S.H. Kim, Acoustical analysis of multiple cavities connected by necks in series with a consideration of evanescent waves, *Journal of Sound and Vibration* 273 (3) (2004) 515–542.
- [23] M.K. Au-Yang, Free vibration of fluid-coupled coaxial cylindrical shells of different lengths, *Transactions of ASME/Journal of applied mechanics* 43 (1976) 480–484.
- [24] A.W. Leissa, *Vibration of Plates*, The Acoustical Society of America, 1993.
- [25] L. Meirovitch, *Analytical Methods in Vibrations*, Macmillan Publishing Co. Inc., New York, 1967.
- [26] L. Meirovitch, *Elements of Vibration Analysis*, McGraw-Hill Book Company, New York, 1986.
- [27] Sysnoise rev. 5.5 User's Manual, *LMS International*, Leuven, Belgium, 2000.